5-1-2016

Characterization of the Non-Uniqueness of Used Nuclear Fuel Burnup Signatures through a Mesh-Adaptive Direct Search

Steven Skutnik
University of Tennessee, Knoxville, sskutnik@utk.edu

David R. Davis
University of Tennessee, Knoxville

Recommended Citation

S.E. Skutnik, D.R. Davis, "Characterization of the non-uniqueness of used nuclear fuel burnup signatures through a Mesh-Adaptive Direct Search," Nuclear Instruments and Methods in Physics Research Section A: Accelerators, Spectrometers, Detectors and Associated Equipment, Volume 817, 2016, Pages 7-18, ISSN 0168-9002, https://doi.org/10.1016/j.nima.2016.02.007.

Characterization of the Non-Uniqueness of Used Nuclear Fuel Burnup Signatures through a Mesh-Adaptive Direct Search

Steven E. Skutnik[a,*], David R. Davis[a]

[a]*Department of Nuclear Engineering, University of Tennessee-Knoxville, Knoxville, TN 37996*

Abstract

The use of passive gamma and neutron signatures from fission indicators is a common means of estimating used fuel burnup, enrichment, and cooling time. However, while characteristic fission product signatures such as ^{134}Cs, ^{137}Cs, ^{154}Eu, and others are generally reliable estimators for used fuel burnup within the context where the assembly initial enrichment and the discharge time are known, in the absence of initial enrichment and/or cooling time information (such as when applying NDA measurements in a safeguards/verification context), these fission product indicators no longer yield a unique solution for assembly enrichment, burnup, and cooling time after discharge. Through the use of a new mesh-adaptive direct search (MADS) algorithm, it is possible to directly probe the shape of this "degeneracy space" characteristic of individual nuclides (and combinations thereof), both as a function of constrained parameters (such as the assembly irradiation history) and unconstrained parameters (e.g., the cooling time before measurement and the measurement precision for particular indicator nuclides). In doing so, this affords the identification of potential means of narrowing the uncertainty space of potential assembly enrichment, burnup, and cooling time combinations, thereby bounding estimates of assembly plutonium content. In particular, combinations of gamma-emitting nuclides with distinct half-lives (e.g., ^{134}Cs with ^{137}Cs and ^{154}Eu) in conjunction with gross neutron counting (via ^{244}Cm) are able to reasonably constrain the degeneracy space of possible solutions to a space small enough to perform useful discrimination and verification of fuel assemblies based on their irradiation history.

1. Introduction

The use of passive gamma-ray signatures from characteristic fission products is a staple for non-destructive burnup analysis of used nuclear fuel, both for burnup credit applications (for used

*Corresponding author

Email address: sskutnik@utk.edu (Steven E. Skutnik)

nuclear fuel storage and management) as well as for safeguards and material accountancy applications. In this latter case, passive gamma-ray measurements are typically used as either a gross estimator of nuclear fuel burnup [1–3] (i.e., to reconstruct burnup gradients across assemblies) or are combined with other techniques to verify operator declarations of the assembly irradiation history with the objective of establishing total assembly plutonium content via reconstruction of the assembly isotopic content through depletion simulations with the estimated burnup, such as through the use of depletion codes like ORIGEN (part of SCALE) [4–6]. In this latter case, calculations of the assembly plutonium content rely on estimates of the fuel burnup, enrichment, and cooling time following its last irradiation cycle [7, 8].

Passive gamma measurements of prominent gamma signatures are typically used as burnup and cooling time indicators, such as ^{137}Cs, ^{154}Eu, or ratios of of gamma lines such as the ratio of ^{134}Cs to ^{137}Cs intensity [1–3, 9, 10]. These nuclides are used due to both their well-established relationship with assembly burnup (and in certain cases, cooling time) as well as their relatively prominent gamma signatures capable of being distinguished within the complex spectrum of spent fuel assemblies [9]. Passive non-destructive analysis (NDA) techniques (including both passive gamma spectroscopy and passive measurements of gross neutron counts [1, 11, 12]) offer a preferred pathway for estimating used fuel inventories given that they can be performed relatively quickly and inexpensively compared to destructive analysis techniques and require minimal instrument complexity [13]. As a result, passive gamma signatures analysis continues to serve as a foundation for safeguards technology development efforts such as the Next Generation Safeguards Initiative [10, 14, 15].

Beyond characterization of spent fuel plutonium content, passive gamma NDA indicators are likewise frequently cited as a means of establishing a unique "fingerprint" for assemblies, including for cases such as re-establishing continuity-of-knowledge upon a loss of on-site power [8] or for termination of safeguards at a geological repository [12]. In these types of applications, measurements would ideally be able to uniquely verify operator declarations on the basis of passive signatures; however, as a practical matter, such systems are typically oriented around the ability to verify (or reject) operator declarations (such as cycle when of an assembly was discharged or its discharge burnup). For example, assuming typical cycle lengths on the order of 12-18 months, an uncertainty of less than ± 1 year would be expected to discriminate between discharge cycles. Similarly, NGSI has expressed a goal of characterization of plutonium within assemblies within $\pm 5\%$ [14, 15], which

roughly corresponds to the same level of uncertainty in discharge burnup.

Unique determination of assembly initial enrichment is more challenging and is typically considered beyond the means of passive NDA techniques alone [16]; however other researchers have claimed to make unique discrimination of the initial enrichment by employing semi-empirical relationships between burnup and initial enrichment based on the assumption that nuclear plant operators would seek to minimize operating margins [17]. While relying on estimates of cooling time and discharge burnup would allow safeguards inspectors to narrow down an assembly to within a discharged batch of assemblies (given a sufficiently tight tolerance on these parameters), the ability to independently establish an assembly's initial enrichment (or at the very least to discriminate between different potential fuel enrichments within a single batch, where differences can range on the order of 1-3% ^{235}U) is still potentially required to provide unique identification of assemblies.

In an ideal circumstance, a truly accurate reconstruction of isotopic inventories would rely on information provided directly from the reactor operator. However, given that a goal of safeguards measurements is to independently verify operator declarations, measurements from the fuel must serve to act as a proxy for the fuel parameters required to accurately reconstruct the assembly isotopic content. Assuming that the concentrations of burnup indicator nuclides are unique to the specific combination of fuel enrichment, burnup, and cooling time, the total plutonium inventory within the assembly is therefore also unique. Similarly, given a specified limiting measurement precision σ_N, it follows that the space of plutonium inventories would likewise show some statistical uncertainty σ_{Pu}, proportional to the measurement uncertainty in burnup.

However, while characteristic fission product signatures such as ^{134}Cs, ^{137}Cs, ^{154}Eu, and others are generally reliable estimators for used fuel burnup within the context where the assembly irradiation history is well-known, prior work by Cheatham and Francis has indicated that the space of solutions based on burnup indicators is in fact not unique for the space of initial fuel enrichment, burnup, and cooling time indicators [18]. Rather, they observed that a phase space of non-unique combinations of reactor parameters exist, wherein the inventories of burnup indicator nuclides are effectively indistinguishable from one another. Put another way, there exists a non-trivial space in the enrichment, burnup, and cooling time domains that yield the same inventories of burnup indicator nuclides within some measurement tolerance σ_N. Therefore, the same measured burnup indicator species yields a range of potential plutonium concentrations in the fuel. (Note that while NDA measurements would still uncover gross operator misrepresentations of an assembly's irra-

diation history, such as short-cycling intended to favorably manipulate the ^{239}Pu-to-^{240}Pu ratio, smaller uncertainties in total assembly Pu content are still relevant to contexts such as front-end accountancy measurements for reprocessing facilities.)

A useful consideration for passive burnup signatures analysis for used fuel burnup information in such contexts is therefore the extent of the non-uniqueness of this signature space, i.e. the size of the phase space made up of potential alternative assembly irradiation history characteristics (initial enrichment, burnup, and cooling time) which yield similar gamma signatures and in particular the influence of unconstrained parameters such as the time after discharge before measurement and the achievable measurement uncertainty on key signatures on the size of this phase space.

In this paper, we propose a new method for characterizing the shape of this degenerate signature space through the use of a Mesh Adaptive Direct Search (MADS) algorithm. By coupling the MADS algorithm directly with the latest ORIGEN application program interface (API) [19], it is thus possible to automate the exploration of the phase space shape characteristic of individual nuclides both as a function of a constrained parameters (such as the assembly's initial enrichment and irradiation history) as well as its unconstrained parameters (i.e., time before measurement and measurement uncertainty of individual nuclides). The goal of this work is to evaluate how this "degeneracy space" evolves with particular characteristics such as the nuclide identifier species, cooling time, and potential combinations of nuclide measurements that can be used to constrain the shape of the space (thereby limiting the uncertainty in calculated plutonium content).

2. Theory and methods

The objective of this method to determine the potential size of a group of ambiguous solutions (phase space), within which the concentrations of all indicator nuclides vary within a given tolerance ($\pm\sigma_N$). For example, if the only indicator nuclide is ^{137}Cs and $\sigma_{137} = \pm 5\%$, the phase space will be the group of solutions which contain a ^{137}Cs concentration within 95%–105% of the ^{137}Cs concentration in the nominal case, regardless of the concentrations of other nuclides. This tolerance accounts for the uncertainty inherent in any measurement method.

To find the phase space for arbitrary indicator nuclides and thresholds, we created a tool called OrigenDSA, or the ORIGEN Degenerate Signatures Analysis. The OrigenDSA tool builds directly upon the new ORIGEN API (to be be released as part of SCALE 6.2) [19] in order to efficiently harness ORIGEN for performing depletion calculations. Here, the search for degenerate assembly

history parameters is performed via a mesh-adaptive direct search algorithm (MADS), which treats the group of all possible solutions as a three-dimensional space, refining the interesting solutions until the phase space appears as a solid shape embedded in the search space.

2.1. Estimation of used fuel burnup from passive gamma / neutron signatures

Gamma rays emitted from used fuel assemblies are the product of specific fission product decays. By counting the number of photons emitted (and making the appropriate efficiency corrections), the gamma ray intensity can be correlated to the inventory of the fission product species in question as follows (Equation 1) [9]:

$$I = \epsilon \kappa S N \lambda e^{-\lambda t} \tag{1}$$

Where:

- I = gamma ray count rate (cps)
- ϵ = absolute detection efficiency (including self-attenuation of gammas within the fuel, detector solid angle, and detector intrinsic efficiency)
- κ = decay line branching ratio ($\frac{\gamma}{\text{decay}}$)
- N = number of fission product nuclei (atoms)
- λ = fission product decay constant ($\frac{\text{decays}}{\text{nucleus} \cdot \text{sec}}$)
- t = cooling time before measurement (seconds)

Similarly, because the dominant spontaneous fission neutron source term in spent fuel is ^{244}Cm, passive neutron counting is therefore treated as roughly proportional to the total ^{244}Cm content of the fuel. Gross neutron counting thus provides a separate means of estimating used fuel burnup [11, 12]. The intensity of the passive neutron source term (itself the product of several neutron captures) is generally estimated through empirical relationships as being approximately proportional to burnup to the fourth power [1, 9, 12].

The basic premise of fission product burnup indicators is that the relationship between the fission product identifier can be well-correlated with burnup; this is best illustrated as the near-linear relationship between ^{137}Cs and the ^{134}Cs to ^{137}Cs ratio, as shown in Figure 1.

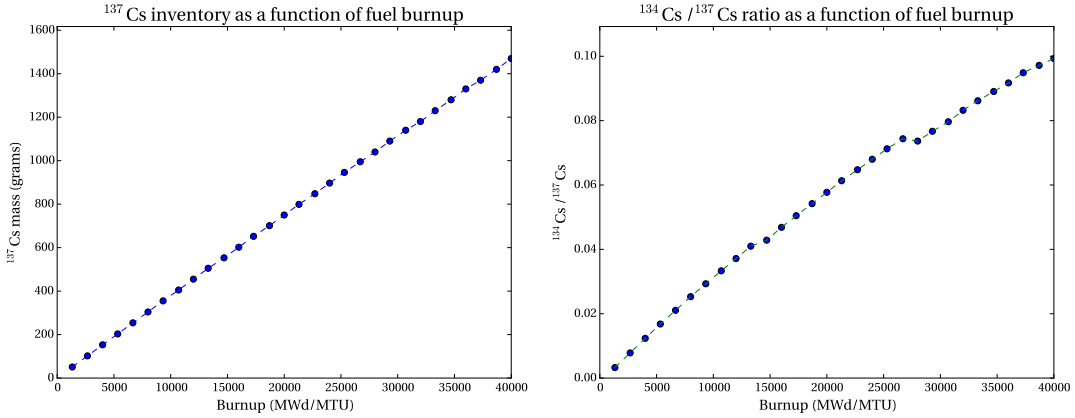

(a) ^{137}Cs inventory as a function of burnup (b) Ratio of ^{134}Cs to ^{137}Cs as a function of burnup

Figure 1: Relative inventory of ^{137}Cs and ratio of ^{134}Cs to ^{137}Cs as a function of fuel burnup (calculated with ORIGEN [5]); arbitrary units of concentration. Note the near-linear relationship of of both as a function of burnup. Discontinuities in the ^{134}Cs / ^{137}Cs ratio are due to 30-day inter-cycle decay periods.

For ^{137}Cs and ^{133}Cs (the stable precursor to ^{134}Cs), the accumulated fission yield is approximately equal from ^{235}U and ^{239}Pu (c.f. Figure 2), thus making these nuclides a good proxy to the total number of fissions in the fuel (assuming an appropriate correction for decay time). In other cases (e.g., ^{106}Ru), the measured fission product indicator is highly *divergent* for U/Pu fission, thereby allowing for a discrimination in the number of fissions arising from ^{235}U and ^{239}Pu, which can serve as another useful indicator of burnup (as well as being correlated to initial enrichment). One will observe that nearly all of the major burnup indicators are located near the yield maxima of the of the bifurcated fission yield distribution (as shown in Figure 2), thereby ensuring that the signatures from these nuclides can be resolved within the complex spent fuel gamma spectrum.

For certain isotopic indicators (such as ^{134}Cs, ^{154}Eu and ^{244}Cm), the isotopic inventory is directly proportional to the number of neutron absorptions rather than the number of fissions directly (therefore being proportional to total thermal neutron flux, and thus still roughly correlated with burnup). Further, with the exception of ^{244}Cm, each of these nuclides has a prominent gamma signature that can easily be resolved above the Compton background in spent fuel (implying both sufficient yield, branching ratio intensity, and gamma energy of the decay line) [9]; a comprehensive list of common burnup indicator nuclides is presented in Table 1.

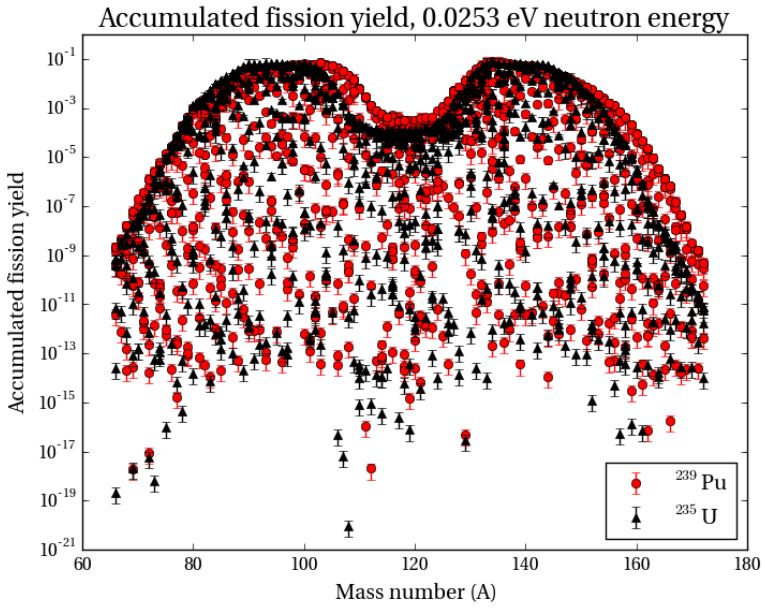

Figure 2: Accumulated fission yields from thermal fission (E = 0.0254 eV) for ^{235}U and ^{239}Pu, adapted from ENDF/B-VII.1 cumulative fission yield data [20].

Upon estimating the fission product species inventory, this can then be correlated back to the burnup of the fuel zone being measured as Equation 2 [9]:

$$\% \text{ burnup} = 100 \cdot \frac{N/Y}{U} \tag{2}$$

Where:

- N = fission product nuclei (atoms)
- Y = effective fission product yield
- U = initial number of uranium atoms

Thus, for purposes of this analysis, it is assumed that by calculating the number of fission product atoms directly in depleted fuel, this serves as a reasonable proxy to measured fission product indicator concentrations (i.e., given a prior, known relationship between the fission product species and the total fuel burnup). Further, it is assumed that given a measurement uncertainty σ_N for a particular fission product isotope (based on the detection efficiency), fission product inventories

Table 1: Half-lives and prominent gamma peaks of key burnup indicator nuclides; adapted from [9]; fission yield ratios calculated from ENDF/B-VII.1 fission yield sublibrary [20], gamma energy and yield data from [21]

Nuclide	$\tau_{1/2}$ (y)	κ_γ ($\gamma/_{\text{decay}}$)	E_γ (keV)	Accumulated fission yields		
				^{235}U	^{239}Pu	Yield ratio
^{106}Ru (^{106}Rh)	1.023	0.0993 0.0156	621.93 1050.41	4.015E-3 ± 5.622E-5	4.350E-2 ± 8.700E-4	0.09232[a]
^{134}Cs	2.06	0.9762 0.8546	604.72 795.86	6.699E-2 ± 2.345E-4	0.07016 ± 0.0003508	0.9548[b]
^{137}Cs	30.17	0.8510	661.66	6.188E-2 ± 3.094E-4	6.607E-2 ± 3.304E-4	0.9366
^{144}Ce (^{144}Pr)	0.780	0.01342	696.51	5.450E-2 ± 2.750E-4	3.739E-2 ± 1.870E-4	1.4706[c]
^{154}Eu	8.59	0.1048 0.1801 0.348	996.3 1004.8 1274.43	1.583E-3 ± 2.168E-4	3.613E-3 ± 2.168E-4	0.4381[d]

[a] Accumulated yields reported for ^{106}Rh

[b] Accumulated yields reported for ^{133}Cs (stable)

[c] Accumulated yields reported for ^{144}Pr

[d] Accumulated yields reported for ^{153}Eu (stable)

falling within $\pm\sigma_N$ are effectively "indistinguishable" from the "true" depletion history. These two assumptions form the basis of the analysis carried out in this paper.

2.2. Mesh-adaptive direct search algorithm

Mesh Adaptive Direct Search (MADS), as originally proposed by Audet and Dennis [22], is a derivative-free optimization technique designed to minimize a nonsmooth function $f : \mathbb{R} \rightarrow \mathbb{R} \bigcup \{0, +\infty\}$ where $x \in \Omega \neq \varnothing \subseteq \mathbb{R}^n$. Here, Ω is defined as a "feasible region" of the problem space. For example, for this problem, Ω is defined as the space of combinations of assembly enrichment, burnup, and cooling time which would produce a nuclide concentration within a range of the nominal value (e.g., a ^{137}Cs concentration within 5% of the nominal value). In the general

formulation, for each iteration k, MADS consists of search and poll steps to generate a set of of trial points within a mesh. Each of these trial points is then evaluated first as to whether it lies within the feasibility space Ω, and if so, is evaluated to calculate an objective response f_Ω. The mesh is then preferentially refined toward solutions which produce a lower functional response to the objective function and the search and poll step is repeated until the mesh size parameter Δ_k^m reaches a convergence criteria. In this way, MADS can determine a solution which provides a global minimum to a set objective function, such as the residual between an observed and calculated response.

MADS has been previously applied inverse problems in radiation transport and the detection of special nuclear material (SNM), such as determining an globally optimal solution for shielded source systems [23]. For this class of problem, the chief advantage of MADS is in its strong convergence properties; while other optimization techniques (such as Levenberg-Marquardt) are sensitive to initial parameter guesses and do not always locate the global optima (for this case, solution for uranium enrichment which minimized the residual between the calculated and actual gamma-ray emissions from a shielded source), MADS was found to reliably locate the global optimum even with initial parameter guesses relatively far from the true solution [23].

However, unlike the general case of optimization of nonsmooth problems as proposed by Audet and Dennis (and likewise employed to inverse radiation transport problems by Armstrong and Favorite [23]), here within this study the goal is not to determine a solution that *minimizes* a residual between an observed response and the solution observed through a parameter space search, but rather to characterize the *shape* of all feasible solutions which match a particular objective function (i.e., parameter combinations of assembly enrichment, burnup, and cooling which produce nuclide inventories within a specified tolerance). Here, the application of MADS is thus to define the feasible *boundary* of the solution space (i.e., determining the shape of Ω for a given nuclide or combination of nuclides), rather than to locate a global optimum for a measured assembly's initial enrichment, burnup, and cooling time given a measured nuclide response. With this different aim in mind, the approach taken herein still employs a similar iterative mesh refinement strategy, only in this case seeking to refine the mesh around the solution space boundary rather than the minimum of the response function residual.

In order to understand the use of the mesh-adaptive direct search algorithm for identifying the space of degenerate used fuel burnup signatures, it is useful to start with a simple demonstration

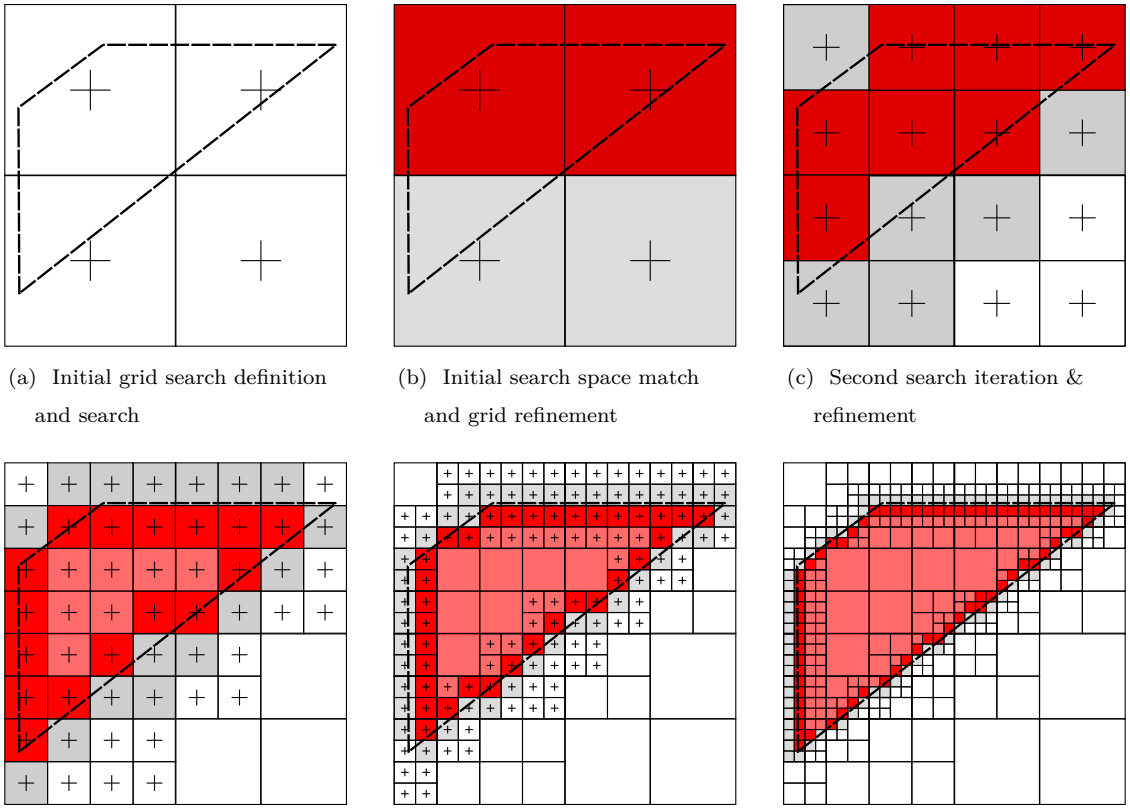

(a) Initial grid search definition and search

(b) Initial search space match and grid refinement

(c) Second search iteration & refinement

(d) Third search iteration & refinement

(e) Fourth search iteration & refinement

(f) Fifth search iteration & refinement

Figure 3: Example of a mesh-adaptive direct search, applied to a two-dimensional phase space. The "true" matching space is marked with a dashed black line. Nodes are searched from the center of the space; matching nodes (red) and non-matching "neighbor" nodes (gray) are divided and refined. Non-matching, non-neighbor (exterior non-match, white) nodes are not refined, nor are matching nodes entirely surrounded by other matching nodes (interior match, pink).

to illustrate the basic principle, shown in Figure 3. The MADS algorithm employed for this study consists of two basic operations: testing mesh nodes for matches (in this case, matching concentrations of particular nuclides within a tolerance $\pm\sigma_N$) and mesh refinement. In the mesh node testing phase, the center of each node to determine whether the concentration matches within the tolerance σ_N; if it does, the node is marked as `true`; otherwise it is marked `false`. For searches involving more than one nuclide, the search is assumed to be a logical `AND` operation, wherein all nuclides

must match within the specified tolerance (set independently for each nuclide) for the search result to return `true`; otherwise if any individual nuclide falls outside of its tolerance, the node is marked `false`.

Dividing the space along orthogonal dimensions, a coarse mesh is established. After each round of depletion solutions and nuclide comparisons, the set of degenerate solutions is identified (i.e., those sets containing the specified nuclides within a tolerance of $\pm\sigma_N$ of the nominal case) and the mesh is refined according to the following criteria:

1. All nuclides in the case match the nominal case within each individual nuclide tolerance $\pm\sigma_N$, **and** at least one neighboring mesh cell has one or more nuclide that do **not** fall within the tolerance limit **or**
2. At least one nuclide does not match within the tolerances specified, **but** at least one neighboring mesh cell does match within all nuclide thresholds

This process is illustrated for a two-dimensional search shown in Figure 3. Starting with an *a priori* "true" phase space (unknown to the algorithm), the space is divided into an initial search grid (Figure 3a). Nodes whose centers are within the phase space will return a match (red cells in Figure 3b). In the mesh refinement phase, matching nodes (Figure 3b, red) and nodes that are directly adjacent to matching nodes ("neighbor" cells, such as in Figure 3b, gray) will be split for mesh refinement.

In subsequent iterations, exterior nodes that do not match and are not adjacent to matching cells ("exterior" nodes) are dropped from mesh refinement (thus decreasing the total number of nodes to be evaluated in subsequent iterations). Similarly, matching nodes that are completely surrounded by matching nodes on all sides ("interior" nodes, shown as pink in Figure 3d) will likewise not be refined. Here, the goal instead is to refine only those cells which define the edge of the "true" phase space, thus maximizing computational efficiency. Each subsequent iteration (Figures 3e and 3f) progressively refines the shape of the grid until the contours of the phase space are closely traced out. In these later iterations, the gains from eliminating solely interior and exterior nodes from mesh refinements is clear (as these do not further contribute to characterizing the shape of the degeneracy space).

This process is then continuously iterated until a user-specified granularity limit is reached. Through a parallelized implementation, the search can be efficiently scaled to multiple computational nodes (as individual mesh cases are independent of one another). The use of neighbor cell

match states (i.e., refining cells based on the presence of a neighbor cell with an opposite match condition) is done both to enhance computational efficiency (i.e., it being redundant to refine / re-evaluate mesh cells surrounded by matching cases) and to enhance the resolution of the phase space boundaries (i.e., discerning the true boundaries of the degenerate signature phase space).

It should be noted that the mesh-adaptive search approach employed in this investigation (wherein completely enclosed nodes are not refined further for sake of computational efficiency) stands in contrast to the more general MADS approach, both in its focus on the boundaries of the feasible solution space (rather than the global minimum) and in the fact that the approach presented herein assumes a simply-connected solution space (i.e., in which all points within the boundary of the solution are assumed to also satisfy the solution condition with no "holes"). The premise of this assumption is that the production of burnup indicator nuclides is a continuous function of enrichment, burnup, and cooling time (such as shown in Figure 1); therefore the assumption that the space is simply-connected (and the subsequent simplification of the MADS approach employed herein) appears to be warranted. Working from this assumption that the solution space is simply-connected, the primary goal of this work has been to evaluate the shape of the exterior of this solution space, and in particular how it may possibly be constrained through combinations of common indicator nuclides. Thus, based upon this assumption, a mesh refinement strategy centered upon refinement of the outer boundary nodes was chosen in order to efficiently determine the shape of the solution space boundary.

Meanwhile, a drawback of the (modified) MADS approach is that even in dropping solely interior / exterior nodes from the mesh refinement, the number of nodes to be evaluated quickly multiples with each successive iteration. Meanwhile, each evaluation takes approximately the same amount of time (consisting of calls to the ORIGEN API to evaluate the depletion solution at the particular node enrichment, burnup, and cooling time); thus the computational time dramatically increases with each mesh refinement. Therefore, a number of refinement iterations was chosen that would result in a maximum node width of 4% of the search space.

2.3. OrigenDSA search operation

The OrigenDSA MADS algorithm works almost exactly like the search demonstrated in Figure 3, only across three dimensions: initial enrichment, discharge burnup, and cooling time following discharge. (Note that while one could likewise feasibly explore a fourth dimension corresponding

Table 2: Nominal reactor parameters evaluated with OrigenDSA

Parameter	Value
Assembly type	Westinghouse 17x17 (PWR)
Irradiation cycles	3
Cycle length (d)	335
Inter-cycle decay (d)	30
Enrichment†	4.0%
Discharge burnup ($\frac{\text{MWd}}{\text{MTU}}$)†	33,000
Cooling time (d)†	1825‡

† Floating search parameter

‡ Nominal cooling time varies where noted.

to relative moderator density, which is an important parameter for boiling water reactor (BWR) assemblies with an axially-varying void fraction, for purposes of tractability, the scope of this study has been limited exclusively to parameters pertaining to pressurized water reactor (PWR) assemblies.) Each node represents a perturbation of a "nominal" assembly history (defined in Table 2), wherein the nominal parameters are perturbed independently along each search dimension. For each search iteration, the nuclide inventories at each node are checked against those from the "nominal" assembly irradiation history. In addition, the scope of this study has been limited to illustrating the application of the MADS method to exploring the degeneracy space of common burnup indicator nuclides, and as such explores only one nominal burnup / power history scenario. Other scenarios of interest from a safeguards perspective, such as determination of a "short-cycled" assembly for purposes of illicit plutonium production, represent a logical continuation of this work but are likewise beyond the scope of this particular study.

Thus, one can directly probe this degeneracy space through repeated perturbations of a nominal irradiation case using tools such as ORIGEN. In this case, the phase space is broken up into three independent dimensions (initial enrichment, total burnup, and cooling time); it is assumed for this study that other factors such as the power history have a negligible impact. (Other factors, such as void fraction, would be expected to show a substantial impact given the change in the neutron spectral shape; however they were beyond the scope of this study.) Degenerate configurations can

be identified as those having nuclide inventories within the measurement tolerance ($\pm\sigma_N$) for a given nuclide or set of nuclides (i.e., representing the use of measurement ratios such as the ^{134}Cs / ^{137}Cs ratio).

The bounds of the search space are user-configurable and defined relative to the nominal parameters; for example, a burnup space of 33,000 $\frac{\text{MWd}}{\text{MTU}}$ would span from 28,050 $\frac{\text{MWd}}{\text{MTU}}$ to 37,950 $\frac{\text{MWd}}{\text{MTU}}$. Each axis is continuous and can be divided into arbitrarily small intervals, creating an infinite number of testable points; therefore, OrigenDSA begins by partitioning the space into a few relatively large intervals (nodes).

An example of an OrigenDSA search for ^{137}Cs is presented as Figure 4. In the initial search (Figure 4a), a coarse grid is established; this grid is successively refined (Figures 4b and 4c), highlighting the expected burnup-dependent linear slope. Meanwhile, the solution appears to be largely independent of enrichment and cooling time within the specified search space.

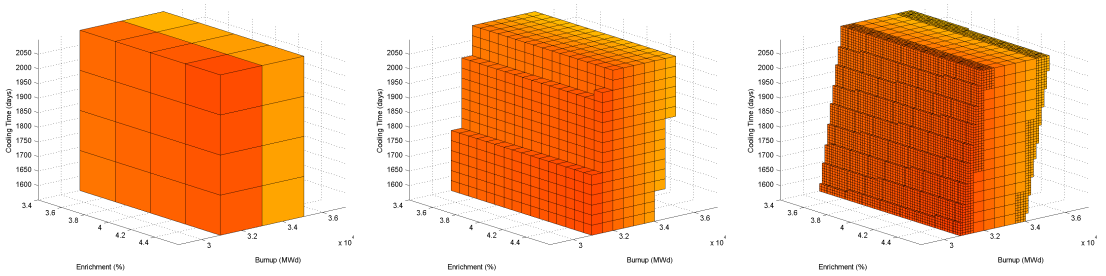

(a) Initial search grid (b) Mesh refinement: iteration 1 (c) Mesh refinement: iteration 2

Figure 4: Degeneracy space resolution over successive search intervals for ^{137}Cs using the OrigenDSA MADS algorithm; $\sigma_{137} = 5\%$

3. Degeneracy space shape characterization for common burnup indicators

3.1. Single-isotope indicators

Figures 5 and 6 show the shape and evolution of the degeneracy space for individual long-lived (^{137}Cs, ^{154}Eu, and ^{244}Cm) and short-lived (^{134}Cs, ^{144}Ce, and ^{106}Ru) burnup indicator nuclides, respectively. Immediately apparent between individual burnup indicator nuclides is the orientation of their degeneracy spaces, which generally take the form of a plane with a thickness corresponding to the measurement tolerance (σ_N). For example, ^{137}Cs is almost exclusively proportional to burnup

alone, admitting a wide range of potential enrichments (3.4–4.5 $^{w}/_{o}$) for a relatively circumscribed burnup range centered about the nominal value (approximately ± 2 $\frac{\text{GWd}}{\text{MTU}}$), while being relatively unconstrained in the cooling time dimension. ^{134}Cs and ^{154}Eu are similar to ^{137}Cs in shape with a slight slope in the enrichment-burnup dimension. ^{244}Cm shows the most radical departure the shape of its degeneracy space, showing a strong orientation along enrichment and burnup, with its plane spanning outward into the cooling time dimension.

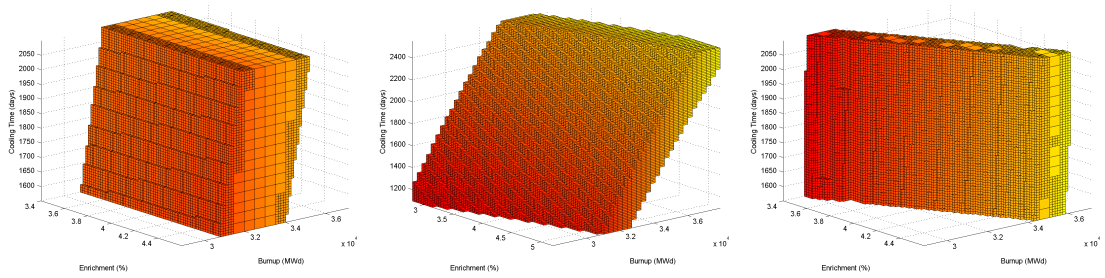

(a) ^{137}Cs: 5 years cooling time; $\Delta_{\text{Pu}} = \pm 15.7\%$.

(b) ^{154}Eu: 5 years cooling time; $\Delta_{\text{Pu}} = \pm 12.0\%$

(c) ^{244}Cm: 5 years cooling time; $\Delta_{\text{Pu}} = \pm 4.7\%$.

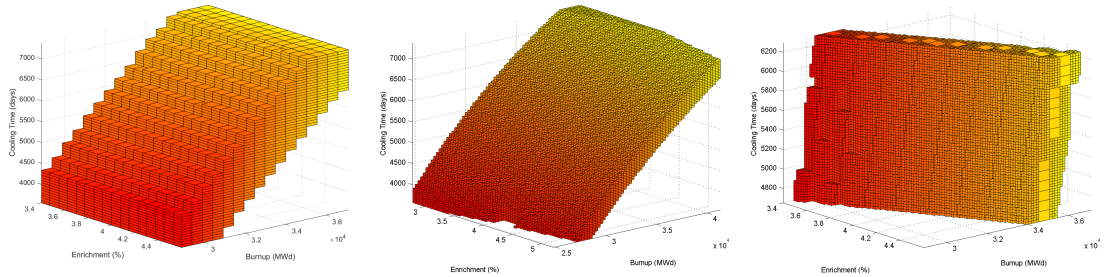

(d) ^{137}Cs: 15 years cooling time; $\Delta_{\text{Pu}} = \pm 9.1\%$.

(e) ^{154}Eu: 15 years cooling time; $\Delta_{\text{Pu}} = \pm 13.1\%$.

(f) ^{244}Cm: 15 years cooling time; $\Delta_{\text{Pu}} = \pm 4.8\%$.

Figure 5: Degeneracy space for longer-lived burnup indicators: ^{137}Cs ($\tau_{1/2} = 30.17$ y), ^{154}Eu ($\tau_{1/2} = 8.59$ y), and ^{244}Cm ($\tau_{1/2} = 18.103$ y); $\sigma_{137} = \sigma_{154} = 5\%$; $\sigma_{244} = 10\%$.

A further analysis of the search space also gives the range of average assembly plutonium content in the space (denoted Δ_{Pu}). For each node in the search space, the total plutonium content is also tallied (denoted by the color map, with darker colors indicating lower plutonium content). The relevance of this metric comes from a safeguards context, in that the non-uniqueness of the burnup signature space likewise implies a range of values for average assembly plutonium content. It thus

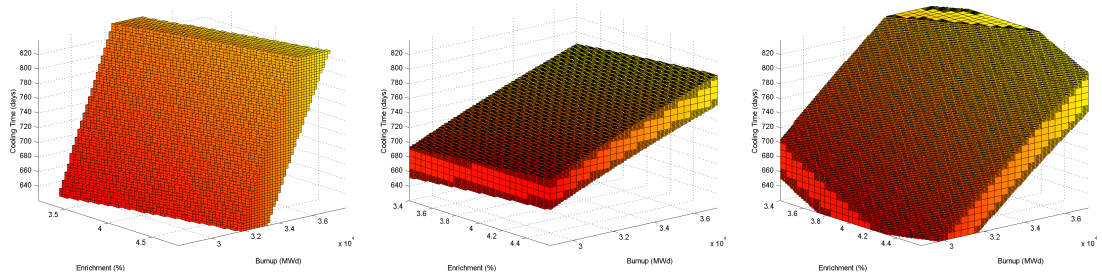

(a) ^{134}Cs: 2 years cooling time. $\Delta_{\mathrm{Pu}} = \pm 15.3\%$.

(b) ^{144}Ce: 2 years cooling time; $\Delta_{\mathrm{Pu}} = \pm 7.85\%$.

(c) ^{106}Ru: 2 years cooling time; $\Delta_{\mathrm{Pu}} = \pm 7.35\%$.

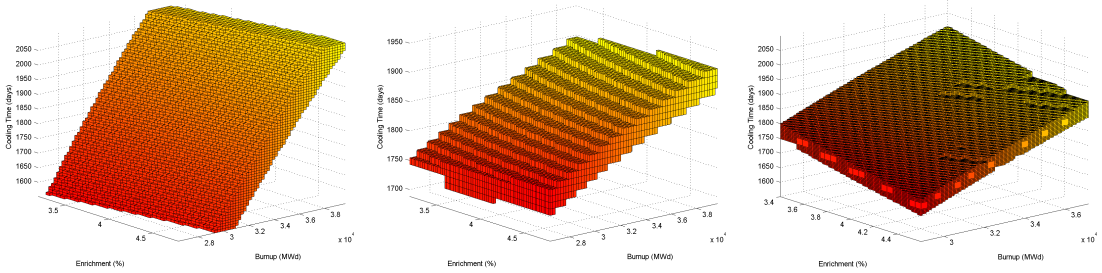

(d) ^{134}Cs: 5 years cooling time. $\Delta_{\mathrm{Pu}} = \pm 8.5\%$.

(e) ^{144}Ce: 5 years cooling time; $\Delta_{\mathrm{Pu}} = \pm 9.15\%$.

(f) ^{106}Ru: 5 years cooling time; $\Delta_{\mathrm{Pu}} = \pm 7.6\%$.

Figure 6: Degeneracy space for shorter-lived burnup indicators: ^{134}Cs ($\tau_{1/2} = 2.06$ y), ^{144}Ce ($\tau_{1/2} = 0.780$ y), and ^{106}Ru ($\tau_{1/2} = 1.023$ y). $\sigma_{134} = \sigma_{144} = \sigma_{106} = 5\%$.

follows that the larger the degeneracy space enrichment, burnup, and cooling time for a given set of burnup signatures, the larger the uncertainty in total plutonium content Δ_{Pu}, although this will be contingent upon the shape of the space as well. (For example, a space highly constrained in burnup but relatively unconstrained in cooling time will show a relatively narrow range in plutonium content compared to the opposite space shape.)

3.2. Constraining the degeneracy space through burnup indicator combinations

As is clear from Figures 5 and 6, single isotopic indicators alone permit a wide range of burnup, enrichment, and cooling time combinations effectively equivalent to those arising from the nominal irradiation history. However, by exploiting shape differences characteristic of each of these nuclides in enrichment, burnup, and cooling time space, it is possible to further constrain the space in such a way to make unique verification of assembly irradiation histories more feasible.

For example, for each of the burnup indicator nuclides, one observes a clear "bend" in the slope of the space as a function of cooling time; i.e., as the original discharged inventories of burnup indicator nuclides decay away, the shape of the degeneracy space evolves with it. This is especially evident for the shorter-lived nuclides (such as ^{106}Ru and ^{144}Ce), which are almost totally unconstrained in the enrichment-burnup plane while showing a strong coupling between burnup and cooling time. The differences in decay rates between indicator nuclides (and thus the evolution of the shape of the individual nuclide degeneracy spaces) thus affords the ability to combine nuclide measurements in order to evaluate the assembly cooling time (as is commonly done with the ^{134}Cs to ^{137}Cs ratio). This principle is illustrated quite clearly in Figure 7 for ^{134}Cs, ^{137}Cs, and ^{154}Eu.

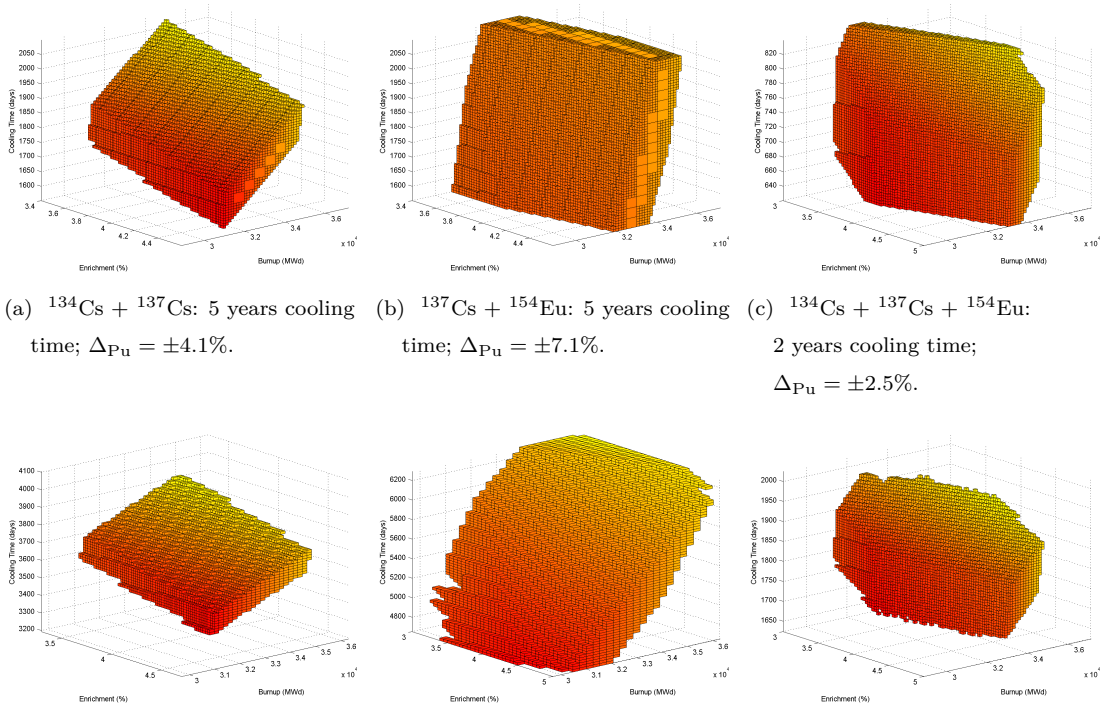

(a) ^{134}Cs + ^{137}Cs: 5 years cooling time; $\Delta_{\mathrm{Pu}} = \pm 4.1\%$.

(b) ^{137}Cs + ^{154}Eu: 5 years cooling time; $\Delta_{\mathrm{Pu}} = \pm 7.1\%$.

(c) ^{134}Cs + ^{137}Cs + ^{154}Eu: 2 years cooling time; $\Delta_{\mathrm{Pu}} = \pm 2.5\%$.

(d) ^{134}Cs + ^{137}Cs: 10 years cooling time; $\Delta_{\mathrm{Pu}} = \pm 7.1\%$.

(e) ^{137}Cs + ^{154}Eu: 15 years cooling time; $\Delta_{\mathrm{Pu}} = \pm 5.2\%$.

(f) ^{134}Cs + ^{137}Cs + ^{154}Eu: 5 years cooling time; $\Delta_{\mathrm{Pu}} = \pm 2.6\%$.

Figure 7: Degeneracy space for the intersections of ^{134}Cs, ^{137}Cs, and ^{154}Eu; $\sigma_{134} = \sigma_{137} = \sigma_{154} = 5\%$

Immediately evident from Figure 7 is the way in which strategic combinations of isotopes (such as ^{134}Cs to ^{137}Cs, seen in Figures 7a and 7d) serve to limit (although not fully constrain) the space

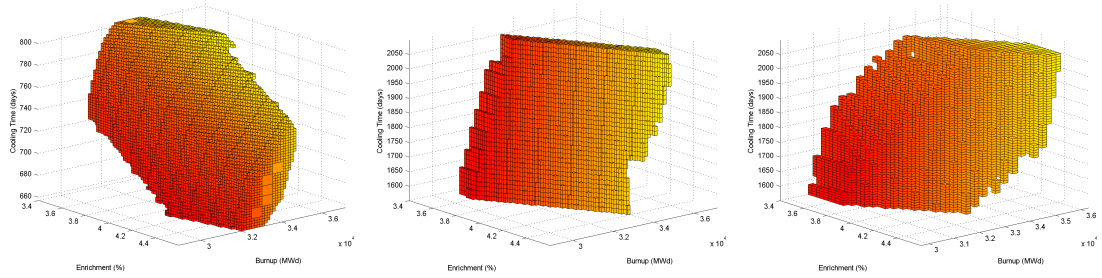

(a) ^{137}Cs + ^{134}Cs + ^{106}Ru: 2 years cooling time; $\Delta_{\mathrm{Pu}} = \pm 3.1\%$.

(b) ^{137}Cs + ^{244}Cm: 5 years cooling time; $\Delta_{\mathrm{Pu}} = \pm 2.7\%$.

(c) ^{137}Cs + ^{154}Eu + ^{244}Cm: 5 years cooling time; $\Delta_{\mathrm{Pu}} = \pm 2.9\%$.

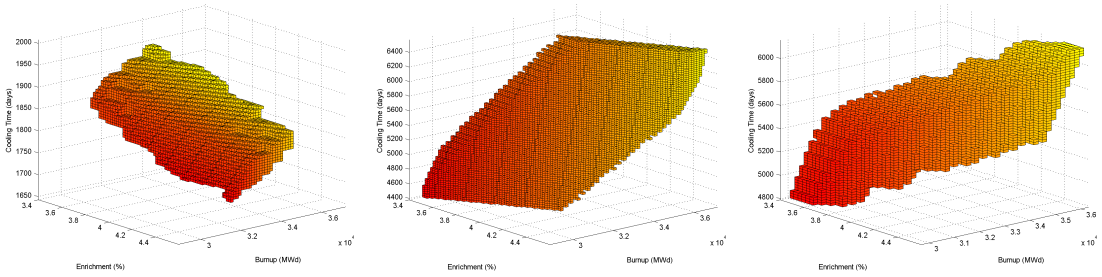

(d) ^{137}Cs + ^{134}Cs + ^{106}Ru: 5 years cooling time; $\Delta_{\mathrm{Pu}} = \pm 3.5\%$.

(e) ^{137}Cs + ^{244}Cm: 15 years cooling time; $\Delta_{\mathrm{Pu}} = \pm 4.1\%$.

(f) ^{137}Cs + ^{154}Eu + ^{244}Cm: 15 years cooling time; $\Delta_{\mathrm{Pu}} = \pm 3.7\%$.

Figure 8: Degeneracy space for the intersections of ^{137}Cs with ^{244}Cm, ^{134}Cs, and ^{106}Ru; $\sigma_{137} = \sigma_{134} = \sigma_{106} = 5\%$, $\sigma_{244} = 10\%$.

of possible enrichment, burnup, and cooling time combinations. The addition of a thrid indicator, ^{154}Eu likewise further constrains the space, namely by taking advantage of the differences in half-lives between the indicator isotopes (thus acting chiefly to reduce the degeneracy space along the cooling time dimension).

In a similar vein, one can exploit these shape differences in the degeneracy space more generally along the dimensions of enrichment and burnup. For example, while ^{137}Cs in particular is especially insensitive to enrichment as a function of burnup (i.e., ^{137}Cs inventories are almost exclusively a function of burnup and cooling time), other nuclides (especially ^{244}Cm) show much more pronounced differences along these dimensions. Thus, the intersection of these nuclides allows one to dramatically reduce the space of potential enrichments, burnups, and cooling times, narrowing

the possible configuration space. This can be seen for the combination of ^{137}Cs and ^{244}Cm (approximating the rough principle of instruments like the Fork detector [11, 12]), such as is shown in Figures 8b and 8e. Here however, an important aspect to note is that the combination of these two signatures is insufficient to provide unique, positive identification of an assembly, given the relatively unconstrained cooling time dimension; at best, such a measurement serves as a *rejection* criteria for gross mismatches along an enrichment / burnup axis (which nonetheless may still prove quite useful for burnup credit applications).

Another common gamma ratio used for burnup estimation is that of $\frac{^{137}\text{Cs}+^{106}\text{Ru}}{(^{134}\text{Cs})^2}$ [1], as seen in Figures 8a and 8d. Here, the space is tightly constrained with respect to burnup (within ± 1 $\frac{\text{GWd}}{\text{MTU}}$) and reasonably constrained in possible cooling times (generally within about ± 150 days); however this measurement alone is insufficient to uniquely identify assemblies on the basis of initial enrichment. Also observable in this space is a linear relationship between the boundary of the cooling time and enrichment (i.e., in which these show a moderate linear anti-correlation). This pattern shifts with longer cooling times (i.e., 5 years, shown in Figure 8d), where the space of possible cooling time shrinks, whereas the space of possible burnups (while still relatively constrained) begins to expand, now showing a linear correlation between burnup and cooling time.

Further, as one observes in Figure 8, the combination of the distinct phase spaces of ^{137}Cs and ^{244}Cm produces a relatively narrow, constrained space with a linear shape along the enrichment and burnup dimensions, limiting the phase space to a narrow strip consisting of possible burnups within a range of approximately $\pm 2,000$ $\frac{\text{MWd}}{\text{MTU}}$of the nominal burnup and enrichments between $\pm 0.4\,(w/o)$. However, because both nuclides are relatively long-lived, the space is relatively unconstrained with respect to cooling time. The addition of other nuclides (such as ^{154}Eu or ^{134}Cs) through basic gamma spectroscopy thus allows a more unique determination of the assembly cooling time alongside enrichment and burnup, seen as Figures 8c and 8f. With the addition of a third, shorter-lived nuclide, the space of non-unique solutions is now small enough to provide useful verification of a particular assembly's declared irradiation history (in that the addition of cooling time thus allows for a narrowing down of possible unique assemblies to the batch and sub-batch level).

What these spaces ultimately reveal is that to uniquely determine an assembly initial enrichment, burnup, and cooling time requires a combination of several nuclide measurements with fundamentally different shape parameters. This includes both gamma and neutron measurements (i.e., ^{137}Cs and ^{244}Cm) along with measurements of specific gamma indicators sensitive to cooling time (i.e.,

nuclides with half-lives appreciably lower than that of ^{137}Cs but long-lived enough to accommodate a range of cooling time intervals before measurement). This latter constraint generally limits the selection of gamma-emitting signatures to those such as ^{134}Cs but more particularly ^{154}Eu. The effect of combining two staggered gamma signatures with neutron counting can be seen in Figures 8c and 8f; the main effect of the addition of a shorter-lived isotope like ^{154}Eu is chiefly in truncating the space of possible discharge dates.

3.3. Burnup indicator combinations for short cooling times

A severe limiting constraint for fuel which has been discharged for longer time periods (>5 years) is the loss of information from short-lived burnup indicators like ^{144}Ce and ^{106}Ru. These short-lived nuclides rapidly decay away, thereby limiting the potential burnup indicator combinations that can be used to constrain the degeneracy space for longer discharge times. Thus, by focusing on a short cooling time interval (2 years post-discharge), it is possible to evaluate the maximum degree to which the degeneracy space is constrained for a given measurement uncertainty of individual nuclides (fixed at 5% for gamma-emitting nuclides and 10% for ^{244}Cm for this study).

While the addition of more gamma-emitting burnup indicator nuclides further narrows the possible space of assembly parameters (such as observed in Figure 9), it is evident that even combinations of all of the most commonly-used gamma-based indicators (e.g. Figure 9e) do not fully constrain the space to a unique solution, or even a solution uniformly centered around the nominal irradiation history. Rather, the trends that emerge appear to show solutions strongly constrained in the cooling time dimension (i.e., generally to within ±30 to ±50 days post-discharge, or about 4–7%) but which indicate a strong linear correlation between initial enrichment and discharge burnup. Such a correlation is consistent across gamma-emitting nuclides such as ^{137}Cs, ^{134}Cs, and ^{154}Eu at longer times post-discharge (c.f., Figures 5 and 7).

In as much, the addition of a more orthogonal signature, such as arising from neutron measurements from ^{244}Cm may prove useful, such as shown in Figure 10. Here, the addition of a neutron-based signature appears to further tighten the bounds of the space compared with gamma-based signatures alone. However even here a linear relationship nonetheless persists between the initial enrichment and discharge burnup, albeit to relatively tight bounds on both (i.e., to within ± 0.4 $^{w}/_{o}$ ^{235}U and ± 2 $\frac{\text{GWd}}{\text{MTU}}$). While not sufficient on its own to uniquely identify an individual assembly discharged from the core, it is nonetheless likely sufficient to independently confirm or

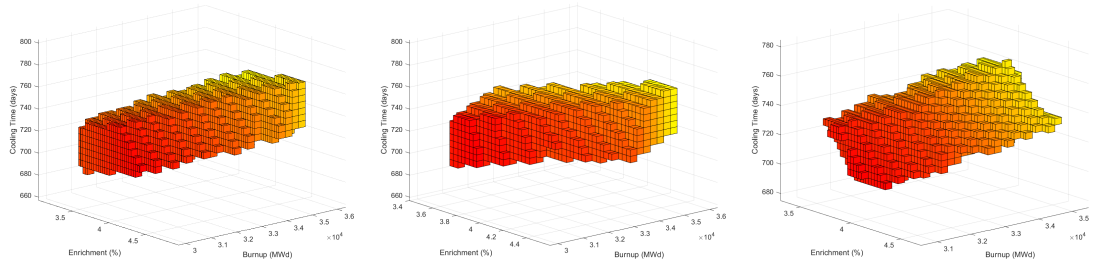

(a) ^{137}Cs + ^{134}Cs + ^{144}Ce; $\Delta_{\mathrm{Pu}} = \pm 2.7\%$.

(b) ^{137}Cs + ^{134}Cs + ^{144}Ce + ^{154}Eu; $\Delta_{\mathrm{Pu}} = \pm 2.2\%$.

(c) ^{137}Cs + ^{134}Cs + ^{144}Ce + ^{106}Ru; $\Delta_{\mathrm{Pu}} = \pm 2.6\%$.

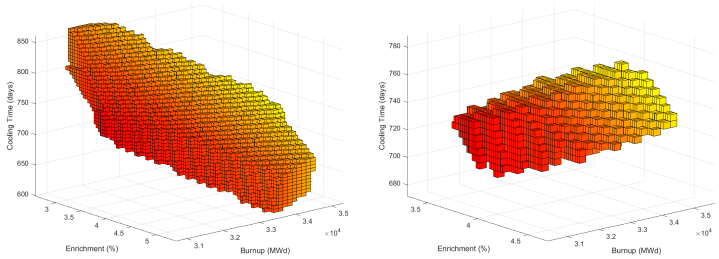

(d) ^{137}Cs + ^{134}Cs + ^{106}Ru + ^{154}Eu; $\Delta_{\mathrm{Pu}} = \pm 2.1\%$.

(e) ^{137}Cs + ^{134}Cs + ^{144}Ce + ^{106}Ru + ^{154}Eu; $\Delta_{\mathrm{Pu}} = \pm 2.2\%$.

Figure 9: Degeneracy spaces for gamma-based burnup indicators, 2 years post-discharge.

reject an operator declaration.

An important takeaway however is in what the marginal benefit gained from the addition of multiple gamma-emitting signatures is in the case of relatively recently-discharged fuel compared with more gross approaches (i.e., relying primarily on ^{137}Cs along with ^{244}Cm, similar to Figure 8b). The primary effect of the addition of more gamma-emitting nuclides (in practical terms, the incorporation of passive gamma spectroscopy capabilities) is primarily in the ability to determine the time of assembly discharge with relatively good precision; these short-lived nuclides (e.g., ^{144}Ce and ^{106}Ru) contribute little in the way of resolving initial enrichment or further determination of discharge burnup beyond what ^{137}Cs and ^{244}Cm are able to provide. Recalling Figure 6, these shorter-lived nuclides primarily serve a chronometric function (contrasted with ^{137}Cs's relatively pure indication of burnup). Thus in the context of the problem of degenerate burnup signatures,

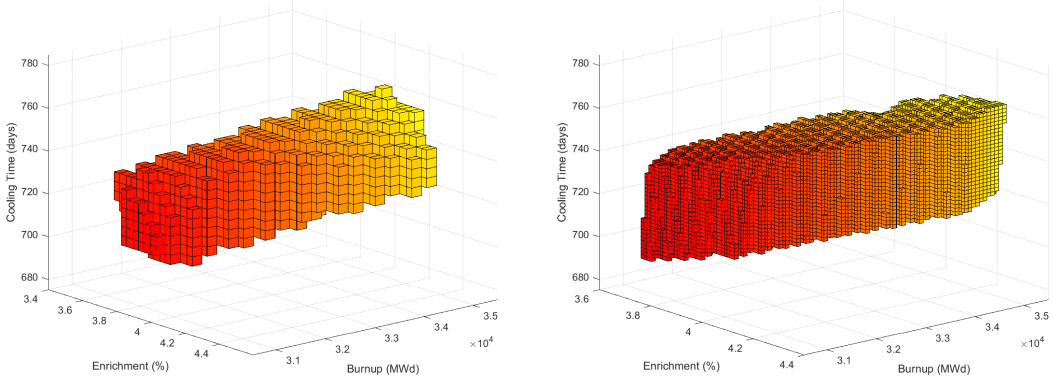

(a) ^{137}Cs + ^{134}Cs + ^{144}Ce + ^{106}Ru + ^{244}Cm: 2 years cooling time; $\Delta_{\mathrm{Pu}} = \pm 2.5\%$.

(b) ^{137}Cs + ^{134}Cs + ^{144}Ce + ^{154}Eu + ^{244}Cm: 2 years cooling time; $\Delta_{\mathrm{Pu}} = \pm 2.2\%$.

Figure 10: Degeneracy spaces for gamma-based burnup indicators, combined with gross neutron counting from ^{244}Cm; 2-years post-discharge. $\sigma_\gamma = 5\%$, $\sigma_{244} = 10\%$.

nuclides like ^{144}Ce and ^{106}Ru are primarily useful in narrowing down the space of discharge times sufficiently to verify operator declarations when combined with other corroborating data (e.g., batch loading schedules).

Finally, not shown is the search space for all indicator nuclides (^{137}Cs + ^{134}Cs + ^{144}Ce + ^{106}Ru + ^{154}Eu + ^{244}Cm, where $\Delta_\gamma = 5\%$ and $\Delta_n = 10\%$) at 2 years post-discharge. This rather extreme case was the only one investigated which yielded a singular, unique solution (wherein no degenerate parameter combinations were found). Such a solution suggests that under very limited circumstances, the initial enrichment, burnup, and cooling time can be determined; however, such a case represents a challenge for passive measurement methods, given that it implies the availability of high-resolution gamma spectroscopy capable of making measurements for still relatively high-activity fuel (a somewhat daunting technical challenge), then correlated with neutron-based measurements of the assembly.

4. Conclusions

Through the novel use of a mesh-adaptive direct search on common gamma signatures used for used nuclear fuel burnup analysis, we have demonstrated that in a safeguards applications context, gamma signatures generally assumed to produce unique solutions for burnup can in fact produce

highly degenerate solutions for assembly irradiation parameters. This suggests that approaches based upon multiple orthogonal signatures (including active interrogation techniques) should be employed in cases where initial enrichment and cooling time before measurement are unavailable or are not otherwise independently verified. While in this case only a single nominal power history and limited space of cooling times and measurement tolerances were explored, this technique could easily be extended to further illustrate the combinations of indicator nuclides required to uniquely isolate an assembly's irradiation history.

The issue of non-uniqueness of burnup signatures has direct safeguards implications in that different possible combinations of enrichment, burnup, and cooling time that yield indistinguishable burnup signatures likewise admit a range of possible values for average assembly plutonium content. Thus, the ability to constrain this space thus offers a means of lowering the range of uncertainty in inferred assembly plutonium content when using burnup signatures as a means of estimating plutonium content through depletion-based calculations. This is most apparent in examples such as the combined space of ^{134}Cs + ^{137}Cs + ^{154}Eu (Figures 7c and 7f) as well as ^{137}Cs + ^{154}Eu + ^{244}Cm (Figures 8c and 8f), which show the most constrained overall spaces for the range of plutonium content values.

With respect to the specific development of passive NDA techniques for used fuel measurements, this would imply that while measurements taken through instruments such as the Fork detector (which leverages gross gamma and neutron counts to estimate burnup) do a reasonable job of constraining an assembly's degeneracy space to a plane oriented across the enrichment and burnup dimensions (i.e., wherein a linear relationship appears to emerge between possible enrichment and burnup values). However, such a measurement is on its own incapable of uniquely identifying assemblies in terms of their initial enrichment or even discharge time. The inclusion of additional gamma signatures (i.e., through spectroscopic measurements) provides some marginal benefits in narrowing the inherent uncertainty in potential assembly plutonium masses, however a limiting factor here is that very few of the common gamma-emitting burnup indicator nuclides are present after more than 10-15 years following discharge (i.e., generally only ^{137}Cs, ^{154}Eu, and ^{244}Cm remain), thus limiting the ability to uniquely identify assemblies at longer decay times after discharge. However, the inclusion of more detailed gamma spectroscopy to resolve multiple burnup-indicating nuclides (such as ^{106}Ru, ^{144}Ce, ^{134}Cs), when taken in tandem with indicators such as ^{137}Cs and ^{244}Cm, may prove more valuable in uniquely identifying more-recently discharged assemblies from the reactor

core. This is due to the fact that these shorter-lived nuclides are more sensitive to cooling time and thus serve a valuable chronometric function, thereby limiting the space of possible cooling time values and thus lowering the total uncertainty in assembly plutonium content.

Furthermore, the existence of the degeneracy space illustrated in this work has vital implications for safeguards in that it implies an inherent, non-trivial uncertainty in estimated plutonium content from passive measurement techniques, in many cases well exceeding the 5% uncertainty target expressed by efforts such as NGSI [14, 15]. While for combinations of burnup indicator nuclide measurements this uncertainty is generally lower than the uncertainty in plutonium content arising individual nuclide measurements, given the existence of a degenerate parameter space, some uncertainty in the estimated plutonium content is unavoidable. The introduction of physically orthogonal signatures (such as the passive neutron signature from ^{244}Cm) can be quite useful in helping to constrain this uncertainty, but ultimately at longer times following discharge, the paucity of available burnup signatures makes the degeneracy space of used fuel characteristics an unavoidable feature. Further attempts to narrow the uncertainty of assembly plutonium content and to provide unique identification of assemblies therefore necessitates the use of alternative measurement techniques (such as those being investigated by the NGSI campaign) in order to provide lower uncertainties in estimated plutonium content.

Finally, this proposed method affords valuable insight for prioritizing efforts to improve nuclear data and measurement uncertainties, namely by offering a means of evaluating the impact of enhanced sensitivity and reduced uncertainty on the relative size of the potential solution space for used fuel enrichment, burnup, and cooling times.

References

[1] B. B. Bevard, J. C. Wagner, C. V. Parks, and M. Aissa. Review of Information for Spent Nuclear Fuel Burnup Confirmation. Technical Report NUREG/CR-6998, U.S. NRC, December 2009.

[2] Wei-Hua Yan, Li-Guo Zhang, Zhao Zhang, and Zhi-Gang Xiao. Feasibility studies on the burnup measurement of fuel pebbles with HPGe gamma spectrometer. *Nuclear Instruments and Methods in Physics Research A*, 712:130–136, February 2013.

[3] I. C. Gauld and M. Francis. Investigation of Passive Gamma Spectroscopy to Verify Spent

Nuclear Fuel Content. In *Institute of Nuclear Materials Management, 51st Annual Meeting*, July 2010.

[4] ORNL. *SCALE: A Modular Code System for Performing Standardized Computer Analyses for Licensing Evaluations*, ORNL/TM-2005/39, Version 6.1 edition, June 2011. Available from Radiation Safety Information Computational Center at Oak Ridge National Laboratory as CCC-75.

[5] I. C. Gauld, G. Radulescu, G. Ilas, B.D. Murphy, M.L. Williams, and D. Wiarda. Isotopic Depletion and Decay Methods and Analysis Capabilities in SCALE. *Nuclear Technology*, 174(2):169–195, May 2011.

[6] S. E. Skutnik, M. L. Williams, and R. A. Lefebvre. ORIGAMI: A New Interface for Fuel Assembly Characterization with ORIGEN. In *International High-Level Radioactive Waste Management (IHLRWM) 2015*, pages 418–425, Charleston, SC, April 2015.

[7] J. Hu, I. Gauld, J. Banfield, and S. Skutnik. Developing Spent Fuel Assembly Standards for Advanced NDA Instrument Calibration – NGSI Spent Fuel Project. Technical Report ORNL/TM-2013/576, Oak Ridge National Laboratory, February 2014.

[8] S. E. Skutnik, I. C. Gauld, C. E. Romano, and H. R. Trellue. Creating NDA "Working Standards" through High-Fidelity Spent Fuel Modeling. In *Proceedings of the Institute of Nuclear Materials Management, 53rd Annual Meeting*, Orlando, FL, July 2012.

[9] J. R. Phillips. Irradiated fuel measurements. In *Passive Nondestructive Analysis of Nuclear Materials*. Los Alamos National Laboratory, Los Alamos, NM, March 1991.

[10] J. D. Galloway, H. R. Trellue, M. L. Fensin, and B. L. Broadhead. Design and Description of the NGSI Spent Fuel Library with Emphasis on the Passive Gamma Signal. *Journal of Nuclear Materials Management*, XL(3):25–34, Spring 2012.

[11] P. M. Rinard and G. E. Bosler. Safeguarding LWR spent fuel with the Fork detector. Technical Report Report LA-11096-MS, Los Alamos National Laboratory, 1988.

[12] S. Vaccaro, J. Hu, J. Svedkauskaite, A. Smejkal, P. Schwalbach, P. De Baere, and I. C. Gauld. A New Approach to Fork Measurements Data Analysis by RADAR-CRISP and ORIGEN Integration. *IEEE Transactions on Nuclear Science*, 61(4):2161–2168, August 2014.

[13] J. Cheatham and J. Wagner. Review and Ranking of NDA Techniques to Determine Plutonium Content in Spent Fuel. In *Institute of Nuclear Materials Management, 51st Annual Meeting*, July 2010.

[14] S. J. Tobin, H. O. Menlove, M. T. Swinhoe, and M. A. Schear. Next Generation Safeguards Initiative research to determine the Pu mass in spent fuel assemblies: Purpose, approach, constraints, implementation, and calibration. *Nuclear Instruments and Methods in Physics Research Section A: Accelerators, Spectrometers, Detectors and Associated Equipment*, 652(1):73 – 75, 2011.

[15] M. A. Humphrey, K. D. Veal, and S. J. Tobin. The next generation safeguards initiative's spent fuel nondestructive assay project. *Journal of Nuclear Materials Management*, XL(3):6–11, 2012.

[16] W. S. Charlton and M. A. Humphrey. External review of the next generation safeguards initiative's spent fuel nondestructive assay project. *Journal of Nuclear Materials Management*, XL(3):12–17, 2012.

[17] D. Vo, A. Favalli, B. Grogan, P. Jansson, H. Liljenfeldt, V. Mozin, P. Schwalbach, A. Sjöland, S. J. Tobin, H. Trellue, and S. Vaccaro. Determination of initial enrichment, burnup, and cooling time of pressurized-water reactor reactor spent fuel assemblies by analysis of passive gamma spectra measured at the CLAB interim-fuel storage facility in Sweden. In *Proceedings of the Institute of Nuclear Materials Management, 56th Annual Meeting*, July 2015.

[18] J. Cheatham and M. Francis. Determining Spent Nuclear Fuel's Plutonium Content, Initial Enrichment, Burnup, and Cooling Time. In *Institute of Nuclear Materials Management, 52nd Annual Meeting*, July 2011.

[19] S. E. Skutnik, F. Havlůj, D. Lago, and I. C. Gauld. Development of an Object-Oriented ORIGEN for Advanced Nuclear Fuel Modeling Applications. In *International Conference on Mathematics and Computational Methods Applied to Nuclear Science & Engineering (M&C 2013)*, Sun Valley, ID, May 2013.

[20] M.B. Chadwick et al. ENDF/B-VII.1 Nuclear Data for Science and Technology: Cross Sections, Covariances, Fission Product Yields and Decay Data. *Nuclear Data Sheets*, 112(12):2887–2996, 2011. Special Issue on ENDF/B-VII.1 Library.

[21] National Nuclear Data Center. Chart of nuclides database. `http://www.nndc.bnl.gov/chart`.

[22] Charles Audet and J.E. Dennis, Jr. Mesh adaptive direct search algorithms for constrained optimization. *SIAM Journal on Optimization*, 17(1):188–217, 2006.

[23] Jerawan C. Armstrong and Jefferey A. Favorite. Identification of unknown interface locations in a source/shield system using the mesh adaptive direct search method. *Transactions of the American Nuclear Society*, 160:375–377, 2012.